Proc. Natl. Acad. Sci. USA
Vol. 89, pp. 1914–1918, March 1992
Biochemistry

Solution conformation of the major adduct between the carcinogen (+)-*anti*-benzo[*a*]pyrene diol epoxide and DNA

MONIQUE COSMAN*, CARLOS DE LOS SANTOS*, RADOVAN FIALA*, BRIAN E. HINGERTY†, SURESH B. SINGH‡, VICTOR IBANEZ‡, LEONID A. MARGULIS‡, DAVID LIVE§, NICHOLAS E. GEACINTOV‡, SUSE BROYDE¶, AND DINSHAW J. PATEL*||

*Department of Biochemistry and Molecular Biophysics, College of Physicians and Surgeons, Columbia University, New York, NY 10032; †Health and Safety Research Division, Oak Ridge National Laboratory, Oak Ridge, TN 37831; Departments of ‡Chemistry and ¶Biology, New York University, New York, NY 10003; and §Chemistry Department, California Institute of Technology, Pasadena, CA 91125

Communicated by Allan H. Conney, December 4, 1991

ABSTRACT **We have synthesized, separated, and purified ≈10 mg of a deoxyundecanucleotide duplex containing a single centrally positioned covalent adduct between (+)-*anti*-benzo[*a*]pyrene (BP) diol epoxide and the exocyclic amino group of guanosine. Excellent proton NMR spectra are observed for the (+)-*trans-anti*-BP diol epoxide-N^2-dG adduct positioned opposite dC and flanked by G·C pairs in the d[C1-C2-A3-T4-C5-(BP)G6-C7-T8-A9-C10-C11]·d[G12-G13-T14-A15-G16-C17-G18-A19-T20-G21-G22] duplex [designated (BP)G·C 11-mer]. We have determined the solution structure centered about the BP covalent adduct site in the (BP)G·C 11-mer duplex by incorporating intramolecular and intermolecular proton–proton distance bounds deduced from the NMR data sets as constraints in energy minimization computations. The BP ring is positioned in the minor groove and directed toward the 5′ end of the modified strand. One face of the BP ring of (BP)G6 is stacked over the G18 and A19 sugar-phosphate backbone on the partner strand and the other face is exposed to solvent. A minimally perturbed B-DNA helix is observed for the d[T4-C5-(BP)G6-C7-T8]·d[A15-G16-C17-G18-A19] segment centered about the adduct site with Watson–Crick alignment for both the (BP)G6·C17 pair and flanking G·C pairs. A widening of the minor groove at the adduct site is detected that accommodates the BP ring whose long axis makes an angle of ≈45° with the average direction of the DNA helix axis. Our study holds future promise for the characterization of other stereoisomerically pure adducts of BP diol epoxides with DNA to elucidate the molecular basis of structure–activity relationships associated with the stereoisomer-dependent spectrum of mutational and carcinogenic activities.**

Benzo[*a*]pyrene (BP), a ubiquitous environmental pollutant, is metabolized in mammalian cells to highly reactive, mutagenic, and tumorigenic diol epoxide derivatives (the field of carcinogen-DNA adducts is reviewed in refs. 1–3). Their binding to cellular DNA is known to cause mutations (3), including the transformation of protooncogenes to oncogenes (4–6). It is widely believed that mutations can constitute the initial first steps in the complex multistage phenomenon of chemical carcinogenesis (7–10). There are two diastereoisomers of the biologically most important bay region BP diol epoxides (BPDEs), and each of these can be resolved into a pair of enantiomers (11). Of the four stereoisomers, only the (+)-*anti*-isomer 7β,8α-dihydroxy-9α,10α-epoxy-7,8,9,10-tetrahydrobenzo[*a*]pyrene [(+)-*anti*-BPDE; structure **1**] is highly tumorigenic (12, 13). Furthermore, it has been shown that racemic *anti*-BPDE is mutagenic in mammalian cells, with the (+)-*anti*-BPDE isomer inferred to be significantly more mutagenic than the (−)-*anti*-BPDE isomer per DNA adduct formed (14–17). These fascinating differences provide an excellent opportunity for examining the molecular basis of the relationships between DNA adduct structure and biological activity, since only the stereochemical properties of these BPDE compounds are different. Some of the characteristics of BPDE adducts with DNA have been characterized by low-resolution optical spectroscopic techniques (for review, see refs. 18–20).

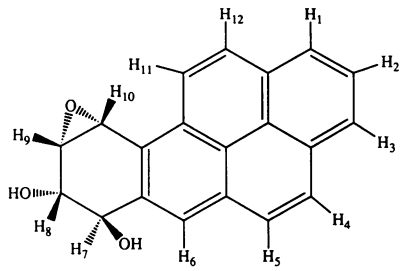

Structure **1**

When reacted with native DNA, (+)-*anti*-BPDE is known to bind predominantly to the exocyclic amino group of deoxyguanosine by trans-addition at the carbon-10 position (21–23). Using methods as described (24, 25), but starting with racemic *anti*-BPDE, we have synthesized ≈5 mg of the stereochemically pure BPDE-oligonucleotide adduct 5′-d[C-C-A-T-C-(BP)G-C-T-A-C-C] where (BP)G denotes the (+)-*trans-anti*-BPDE-N^2-dG adduct (structure **2**). The modified

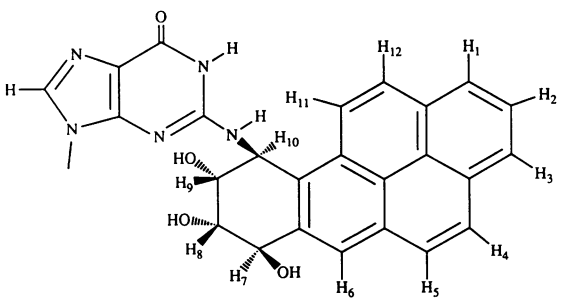

Structure **2**

strand was annealed to its complementary partner strand to generate the (BP)G·C 11-mer duplex (structure **3**), which

BPDE

5′- C1–C2–A3–T4–C5–G6–C7–T8–A9–C10–C11 -3′
3′- G22–G21–T20–A19–G18–C17–G16–A15–T14–G13–G12 -5′

Structure **3**

The publication costs of this article were defrayed in part by page charge payment. This article must therefore be hereby marked "*advertisement*" in accordance with 18 U.S.C. §1734 solely to indicate this fact.

Abbreviations: BP, benzo[*a*]pyrene; BPDE, BP diol epoxide; NOE, nuclear Overhauser effect; NOESY, NOE spectroscopy.

||To whom reprint requests should be addressed.

contains enantiomerically pure (+)-*trans-anti*-(BP)G6 positioned opposite C17 and flanked by G·C pairs. The NMR study was undertaken on 9.6 mg of (BP)G·C 11-mer duplex in 0.4 ml of 0.1 M NaCl/10 mM sodium phosphate, pH 7.0, in H_2O and ^2H_2O. We have combined two-dimensional NMR experiments with computational calculations to define the solution conformation centered about the (BP)G6·C17 modification site in the (BP)G·C 11-mer duplex.

MATERIALS AND METHODS

Preparation of (BP)G·C 11-mer Duplex. The racemic *anti*-BPDE was purchased from the National Cancer Institute Chemical Carcinogen Reference Standard Repository. The yield of the (+)-*trans-anti*-BPDE-N^2-dG 11-mer was 15% starting from racemic *anti*-BPDE. The percentage ratios of (+)-*trans*, (−)-*trans*, (+)-*cis*, and (−)-*cis* adducts in the mixture were 48, 33, 10, and 9%, respectively. The (+)-*trans-anti*-BPDE-N^2-dG 11-mer adduct was easily separable from the corresponding (−)-*trans*, (+)-*cis*, and (−)-*cis* isomeric adducts by preparative HPLC on a C_{18} ODS Hypersil column using a linear 0–90% (vol/vol) methanol/20 mM sodium phosphate, pH 7.0, gradient over a 60-min period as described (24). The nature of the BPDE modification was established by enzyme digestion of the modified oligonucleotide to the mononucleoside level and by comparing the HPLC elution times with those of a (+)-*trans-anti*-BPDE-dG standard. The enzyme digestion studies were carried out with snake venom phosphodiesterase and bacterial alkaline phosphatase. The ratio of C/G/T/A/(BP)G for the modified strand was determined to be 6.0:0:2.2:1.9:0.9. The CD spectra of the modified oligonucleotide and of the adduct isolated from this oligonucleotide are fully consistent with those of the (+)-*trans-anti*-BPDE-N^2-dG adduct standard (26). The modified strand was added to the unmodified strand at 65°C and the stoichiometry was followed by monitoring single-proton resolved resonances in both strands.

NMR Measurements. Two-dimensional nuclear Overhauser effect spectroscopy (NOESY) spectra on the (BP)G·C 11-mer duplex in ^2H_2O buffer at 25°C were recorded at mixing times of 50, 100, 150 and 200 msec. The volume integrals of cross peaks as a function of mixing times were measured to generate the buildup curves. The estimated proton–proton distances were defined by lower and upper bounds using the fixed cytidine H6–H5 2.45-Å separation as the reference distance. As examples, the estimated distance bounds were 2.8–4.8 Å for BP(H11)-G18(H1′) and 2.9–4.5 Å for BP(H10)–G6(H1′).

Two-dimensional correlation spectra on the (BP)G·C 11-mer duplex were recorded in ^2H_2O buffer at 25°C and include phase-sensitive correlated spectroscopy, double-quantum-filtered correlated spectroscopy, and homonuclear Hartmann–Hahn (as a function of spin-lock time) spectra. These experimental through-bond two-dimensional data sets and their simulated counterparts were critical in the assignment of the protons on the BP ring in the (BP)G·C 11-mer duplex.

NMR parameters can be used to distinguish between B-DNA and A-DNA helical conformations (27, 28). The nuclear Overhauser effects (NOEs) between the base proton and its own H2′ proton and the H2″ proton of the 5′-flanking sugar are strong for B-DNA. The NOEs between the base proton and its own H3′ proton and the H2′ proton of the 5′-flanking sugar are strong for A-DNA. The J(1′–2′) vicinal coupling is large for the C2′-*endo* sugar characteristic of B-DNA and small for the C3′-*endo* sugar characteristic of A-DNA. The reverse is true for J(2″–3′) and J(3′–4′) vicinal couplings. These parameters were used in a qualitative manner to distinguish between A- and B-DNA helical conformations for the (BP)G·C 11-mer duplex.

Energy Minimization Computations. DUPLEX is a molecular mechanics program for nucleic acids that performs potential energy minimizations in the reduced variable domain of torsion angle space (29). The vast diminution in the number of variables that must be simultaneously optimized, compared to Cartesian space minimizations, permits large movements from a given starting conformation during minimization. It has the option to include distance contraints through penalty functions to compute structures that are minimum energy conformations (30). Details of the force fields and parametrization are given in ref. 29. Details about the functions employed to search for structures within the NMR-defined distance bounds are given in ref. 31. The penalty functions are released in terminal minimizations to yield unconstrained structures that are energy minima and within the range of the NMR data.

We briefly summarize the search and build procedure as described (32), which was used to generate the energy-minimized structure of the (BP)dG positioned opposite dC in a DNA oligomer duplex. The search began with a modified deoxydinucleoside monophosphate. About 4000 trials were made to survey conformational space. Low-energy conformations from this search were directly embedded in the B-form d(G-C)$_6$·d(G-C)$_6$ 12-mer duplex with energy minimization. Alternately, the dinucleotide conformations were extended to the trinucleotide level with extensive conformational searches for the added residue after which the trimers were embedded in the B-DNA 12-mer duplexes. Details are given in ref. 32. The alternate hydrogen-bonding scheme of the Hoogsteen type at the modification site, which places the carcinogen in the major groove, was also explored, as were possibilities for denaturation at and adjacent to the adduct site. The starting conformation of the (BP)G·C 11-mer duplex was obtained by base sequence and length adjustment of the lowest energy structure for the (+)-*trans-anti*-BPDE-N^2-dG adduct in the alternating d(G-C)$_6$·d(G-C)$_6$ 12-mer duplex. The energy minimization computations to deduce the solution structure of the (BP)G·C 11-mer duplex were based on this starting structure and were guided by the available experimental interproton distances defined by lower and upper bounds that were constrained within the limits using penalty functions.

RESULTS

Exchangeable Proton Spectra. The proton NMR spectrum of the (BP)G·C 11-mer duplex in H_2O buffer at 5°C is plotted in Fig. 1*A*. The observed pattern of narrow and resolved imino protons (12.0–14.0 ppm) and the base and amino protons (7.0–9.0 ppm) establish formation of a single conformation for the (+)-*trans-anti*-(BP)G6 adduct in the duplex. Expanded regions of the NOESY contour plot (mixing time, 200 msec) of the (BP)G·C 11-mer duplex in H_2O buffer at 5°C are plotted in Fig. 1*B*. The NOE cross peaks in these contour plots were analyzed by standard procedures (for review, see refs. 27 and 28) and yielded imino proton assignments including those of (BP)G6 (12.47 ppm) at the modification site, as well as G16 and G18 of flanking G·C pairs. NOEs between guanosine imino and cytidine amino protons are characteristic of Watson–Crick G·C base pairs (Fig. 1*B*, boxed region II), and NOEs between thymidine imino and adenosine H2 protons are characteristic of Watson–Crick A·T base pairs (Fig. 1*B*, boxed region I). The observed NOE patterns establish Watson–Crick pairing at all G·C and A·T pairs, as well as the (BP)G6·C17 pair in the (BP)G·C 11-mer duplex. The N^2-amino proton of (BP)G6 resonates at 8.12 ppm and its down-field shift requires hydrogen-bond participation in the (BP)G6·C17 pair. Chemical-shift ranges for related cytidine amino protons are 8.0–8.5 ppm for the hydrogen-bonded

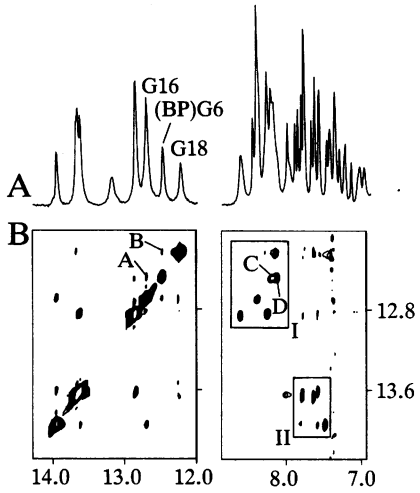

FIG. 1. (*A*) Proton NMR spectrum (12.0–14.0 ppm and 7.0–9.0 ppm) of the (BP)G·C 11-mer duplex in 0.1 M NaCl/10 mM sodium phosphate, pH 7.0, in H_2O at 5°C. The guanosine imino proton assignments for the (BP)G6·C17 modification site and flanking C5·G18 and C7·G16 base pairs are assigned over the spectrum. (*B*) Expanded NOESY (mixing time, 200 msec) contour plot establishing distance connectivities in the symmetrical 12.0- to 14.0-ppm imino proton region (*Left*) and between the imino protons and the 7.0- to 9.0-ppm base and amino proton region (*Right*). The boxed region II shows NOE cross peaks between thymidine imino protons and adenosine H2 protons in Watson–Crick A·T base pairs, and boxed region I shows cross peaks between guanosine imino protons and hydrogen-bonded cytidine amino protons in Watson–Crick G·C base pairs. The cross peaks A to D are assigned as follows: A, (BP)G6(imino)-G16(imino); B, (BP)G6(imino)-G18(imino); C, (BP)G6(imino)-C17(amino); D, (BP)G6(imino)-(BP)G6(amino).

proton and 6.5–7.0 ppm for the exposed proton in a G·C Watson–Crick base pair.

Nonexchangeable Proton Spectra. The proton NMR spectrum of the (BP)G·C 11-mer duplex in ^2H_2O buffer at 25°C is plotted in Fig. 2*A*. The available resolution in the base proton (6.9–8.6 ppm) and sugar H1′ (5.3–6.5 ppm) regions permits resonance assignments using standard through-space and through-bond two-dimensional NMR experiments (33). An expanded NOESY (mixing time, 300 msec) contour plot establishing NOE connectivities between the base and sugar protons in the (BP)G·C 11-mer duplex in ^2H_2O buffer at 25°C is plotted in Fig. 2*B*. The data are of sufficient quality to completely assign the base and sugar (except superpositioned H5′,H5″) protons of all 22 nucleotides in the (BP)G·C 11-mer duplex. The characteristic NOE patterns between the base protons and their own and 5′-flanking sugar H1′ protons for a right-handed duplex (33) are traced for the [T4-C5-(BP)G6-C7-T8]·[A15-G16-C17-G18-A19] central 5-base-pair segment in Fig. 2*B*. The unusually large upfield shift for the H1′ proton of G18 (3.56 ppm) and the smaller upfield shift for A19 (5.14 ppm), along with a similar trend for other protons on these residues (see Fig. 2) requires that the BP ring covalently attached to the G6 modification site stacks predominantly over the sugars of G18 and to a somewhat lesser extent A19 on the partner strand. These results position the BP ring in the minor groove with its long axis directed toward the 5′ end of the modified strand. The sugar rings in the (BP)G·C 11-mer adopt predominantly C2′-*endo* puckers based on a qualitative analysis of NOE and coupling constant patterns.

The BP protons on both the aromatic and nonplanar rings at the (BP)G6 modification site have been assigned in the (BP)G·C 11-mer duplex based on a comparison between experimental and calculated coupling constant patterns and patterns of NOEs between BP protons.

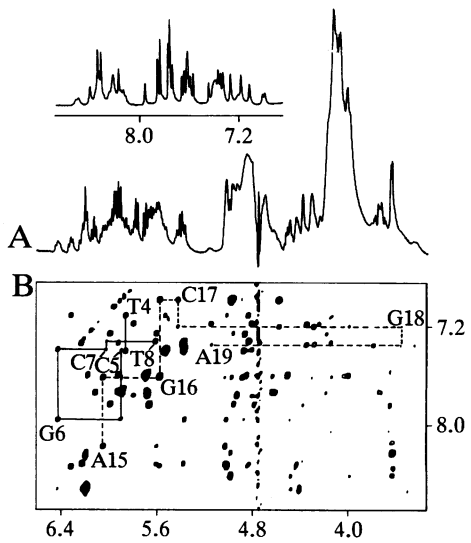

FIG. 2. (*A*) Proton NMR spectrum (6.9–8.6 ppm and 3.4–6.5 ppm) of the (BP)G·C 11-mer duplex in 0.1 M NaCl/10 mM sodium phosphate, pH 7.0, in ^2H_2O at 25°C. (*B*) Expanded NOESY (mixing time, 300 msec) contour plot establishing distance connectivities between the 6.9- to 8.6-ppm base protons and the 3.4- to 6.5-ppm sugar protons. The solid line traces the distance connectivities between the base protons and its own and 5′-flanking sugar H1′ protons in the T4-C5-(BP)G6-C7-T8 segment in the modified strand, and the dashed line follows the connectivities in the A15-G16-C17-G18-A19 segment in the unmodified strand. The BP aromatic protons resonate between 8.1 and 8.5 ppm, and the aliphatic protons resonate between 4.4 and 6.2 ppm. The resonance assignments are based on a comparison between experimental and calculated phase-sensitive and double-quantum-filtered correlated spectroscopy coupling patterns, as well as patterns of NOEs between BP protons. The spectral assignments are as follows: BP(H1,H3), 8.33 ppm; BP(H2), 8.13 ppm; BP(H4,H5), 8.22 ppm; BP(H6), 8.40 ppm; BP(H7), 4.99 ppm; BP(H8), 4.48 ppm; BP(H9), 4.41 ppm; BP(H10), 6.20 ppm; BP(H11), 8.51 ppm; BP(H12), 8.23 ppm. The upfield chemical shift difference on proceeding from the control G·C 11-mer to the (BP)G·C 11-mer for protons on G18 are as follows: H8, 0.65 ppm; H1′, 2.05 ppm; H2′, 1.08 ppm; H2″, 1.87 ppm; H3′, 0.68 ppm; H4′, 0.77 ppm. For protons on A19 the values are as follows: H8, 0.80 ppm; H1′, 1.04 ppm; H2′, 0.39 ppm; H2″, 0.68 ppm; H3′, 0.64 ppm; H4′, 0.79 ppm.

Intermolecular NOEs in (BP)G·C 11-mer Duplex. We have identified and assigned the intermolecular NOEs between the BP and nucleic acid protons in the (BP)G·C 11-mer duplex. These fall into two categories and involve 6 NOEs between the BP aromatic protons and minor groove sugar protons on the G18-A19 segment on the unmodified strand (several of these are shown in Fig. 3*A*) and 11 NOEs between the BP aliphatic protons and the minor groove sugar protons on the (BP)G6-C7 segment on the modified strand (several of these are shown in Fig. 3 *B* and *C*). These intermolecular distance connectivities independently establish that the BP ring is positioned in the minor groove, is directed toward the 5′ end of the modified strand, and stacks over the A18-G19 sugar-phosphate backbone on the unmodified strand.

Energy Minimization Computations. The solution structure of the (BP)G·C 11-mer duplex was deduced by incorporating proton–proton distance constraints obtained from NOE buildup curves in constrained energy minimization calculations using the DUPLEX program (29). The starting conformation of the (BP)G·C 11-mer duplex was obtained by base sequence and length adjustment of a (+)-*trans-anti*-BPDE-N^2-dG adduct in a DNA oligomer deduced from an extensive conformational search with no input experimental constraints (32). A set of NMR-based interproton distances defined by lower and upper bounds between BP protons, between nucleic acid protons, and between BP and nucleic acid protons were constrained within the limits,

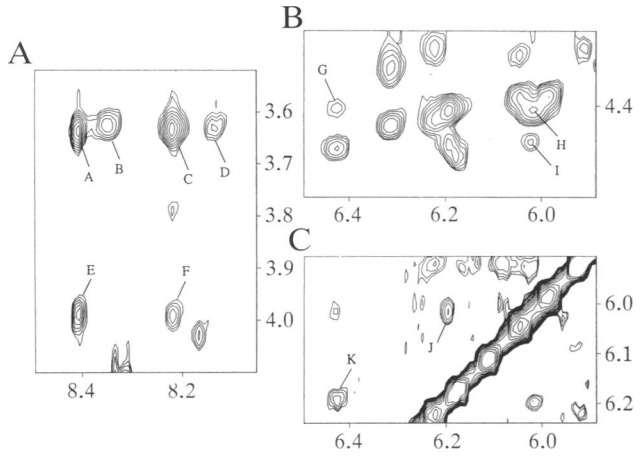

FIG. 3. Expanded NOESY (mixing time, 300 msec) contour plots establishing distance connectivities between the 3.5- to 4.1-ppm and 8.1- to 8.5-ppm regions (*A*), between the 4.1- to 4.6-ppm and 5.9- to 6.5-ppm regions (*B*), and between the 5.9- to 6.2-ppm and 5.9- to 6.5-ppm regions (*C*) in the (BP)G·C 11-mer duplex in 0.1 M NaCl/10 mM sodium phosphate, pH 7.0/^2H_2O at 25°C. The cross peaks A to F are assigned as follows: A, BP(H6)-G18(H4′); B, BP(H1/H3)-A19(H4′); C, BP(H4/H5)-G18/A19(H4′); D, BP(H2)-A19(H4′); E, BP(H6)-G18(H5′/H5″); F, BP(H4/H5)-G18(H5′/H5″). The cross peaks G to K are assigned as follows: G, BP(H9)-G6(H1′); H, BP(H9)-C7(H1′); I, BP(H8)-C7(H1′); J, BP(H10)-C7(H1′); K, BP(H10)-G6(H1′).

using penalty functions (30, 31) during the energy minimization. The parameters used in the current constrained energy minimization guided by distance bounds are the same as those reported in earlier computations with no experimental input (32). The saturated ring of BP was fixed during the constrained energy minimization with the hydroxyl groups in the 7,8-diequatorial-9,10-diaxial conformation reported previously in the crystal structure of the BP tetrol model compound (34) and also observed for (+)-*trans-anti*-BPDE-N^2-dG nucleoside adducts by NMR analysis in solution (26). The observed vicinal coupling constants between the H7 and H8 and between the H9 and H10 protons, as well as 10 NOEs between the aromatic and aliphatic protons, are consistent with this pucker family for the nonplanar ring of BP in the (BP)G·C 11-mer duplex. The structure of the (BP)G·C 11-mer duplex that satisfied the experimental distance constraints was achieved after a single round of energy minimization to convergence. The rms deviation between the starting structure and the constrained energy minimized structure was 0.68 Å for the central d[T4-C5-(BP)G6-C7-T8]·d[A15-G16-C17-G18-A19] 5-base-pair segment of the (BP)G·C 11-mer duplex. Release of all constraints yielded a very similar structure, with rms deviation from the constrained structure of 0.41 Å. Preliminary studies establish that starting structures that differ by 45° in the torsion angles at each of the two bonds at the carcinogen-base linkage site converge to the same final structure after energy minimization guided by the experimental distance bounds.

Solution Structure. Four views of the computed structure for the d[T4-C5-(BP)G6-C7-T8]·d[A15-G16-C17-G18-A19] central segment of the (BP)G·C 11-mer duplex are shown in color in Fig. 4. The BP ring highlighted in yellow is positioned in the minor groove; its long axis is oriented toward the 5′ end of the modified strand with one face in contact with the backbone at residues G18 and A19 on the partner strand. The orientation of the pyrenyl moiety is governed by the two torsion angles at the carcinogen–base linkage site and the pucker of the nonplanar ring, which prevents complete burial in the groove. The torsion angles at the carcinogen–base linkage as defined in ref. 32 are 137° for N1-C2-N2-C10 and 258° for C2-N2-C10-C9 in the (BP)G·C 11-mer duplex. The angle between the long axis of the BP ring and the average

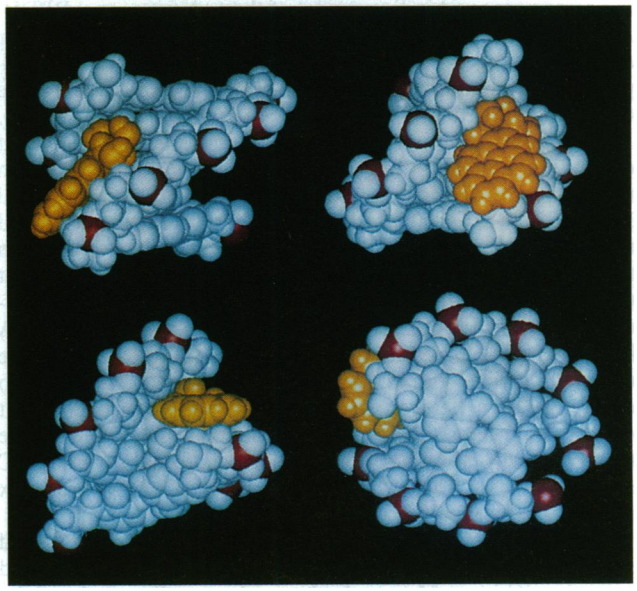

FIG. 4. Four views of the [T4-C5-(BP)G6-C7-T8]·[A15-G16-C17-G18-A19] segment in the solution structure of the (BP)G·C 11-mer duplex. The BP ring (yellow) is positioned in the minor groove and its long axis is directed toward the 5′ end of the modified strand. The upper left view emphasizes the 45° inclination between the BP long axis and the DNA helix axis. The upper right view emphasizes the stacking of the BP ring over the G18-A19 segment on the unmodified strand and the exposed nature of one face of the aromatic ring system of the BP ring. The lower left view is looking into the minor groove. It also emphasizes the differences between the two faces of the BP ring; one face forms van der Waals contacts with the G18-A19 step and the other face is exposed to solvent. The lower right view is down the helix axis. Only a small segment of the BP ring projects beyond the DNA helix diameter. The minor groove width can be measured as the shortest phosphorus–phosphorus separation across the two strands less the 5.8-Å diameter of each phosphorus group. The minor groove width increases on proceeding from the ends of the (BP)G·C 11-mer duplex to the BP adduct site toward the center of the helix. The separations are 4.3 Å for P4-P21 and 4.5 Å for P10-P15 toward either end of the helix and increase to 8.1 Å for P7-P18 toward the center of the helix. (The nomenclature is such that P18 would be the phosphorus at the A18-G19 step.) HELIB 90, available from R. Dickerson (University of California at Los Angeles) was employed to compute these values.

helix axis is ≈45° in the (BP)G·C 11-mer duplex. This value can be compared with angles of 26° (35) and 39° (36) estimated from flow dichroism studies for the (+)-*anti*-BPDE adducts of poly(dG-dC) in solution.

The DNA helix is minimally perturbed by formation of the (+)-*trans-anti*-BPDE-N^2-dG adduct in the computed structure of the (BP)G·C 11-mer duplex. The base pairs adopt Watson–Crick alignment including the (BP)G6·C17 pair at the modification site; all glycosidic torsion angles are in the *anti* range (values distributed between −103° and −125°) and all sugar puckers are in the C2′-*endo* range (pseudorotation phase angle values distributed between 141° and 167°). The backbone torsion angles belong to the B_I-DNA family (37) and the helix remains bent at the adduct site in the computed structure as it was in the starting structure (32). The average helical twist angle for the 5 base pairs centered about the (BP)G6·C17 modification site is 36.3° in the computed structure of the (BP)G·C 11-mer duplex. The minor groove widens at the adduct site (see Fig. 3) to accommodate the BP ring.

DISCUSSION

Structural Conclusions. The present combined NMR and energy minimization computational studies provide strong support for qualitative (38) and quantitative (32) features of

the minor groove binding model of the (+)-*trans-anti*-BPDE-N^2-dG adduct positioned opposite dC in duplex DNA. Our experimental results definitively rule out models that proposed intercalation or wedge-shaped intercalation of the covalently linked BPDE between base pairs in DNA (39, 40). Further, our structure of the (BP)G·C 11-mer complex that directs the covalently attached BP ring toward the 5′ end in the minor groove is in agreement with some computational studies (32, 41) but not with others that direct the ring toward the 3′ end in the minor groove (42–44). Our results differ from the conclusions of computational studies that proposed that the (+)-*trans-anti*-BPDE-N^2-dG adduct can only be positioned in the minor groove of A-DNA (42, 43) since the DNA helix was established in this study to be of the B type for the (BP)G·C 11-mer duplex in solution. Further, we find no evidence for a heterogeneous equilibrium of two different covalently bound BP adduct conformations (35) for the (+)-*trans-anti*-BPDE-N^2-dG adduct positioned opposite dC and flanked by G·C pairs for the (BP)G·C 11-mer duplex reported in this study.

We note several similarities between the present structural study of the (+)-*trans-anti*-BPDE-N^2-dG adduct positioned opposite dC in an 11-mer duplex and an earlier study of the anthramycin-N^2-dG adduct positioned opposite dC in a 6-mer duplex (45, 46). In both cases the covalent adduct adopts a unique alignment in the minor groove with minimal perturbation of the B-DNA helix.

The present study establishes the feasibility of structural studies of enantiomerically pure BPDE adducts covalently attached at single sites in DNA. For the (+)-*trans-anti*-BPDE-N^2-dG adduct positioned opposite dC, the BP is readily accommodated with minimal perturbation in the minor groove of B-DNA. Further, one face of the BP is exposed to solvent and only a small segment of its aromatic ring projects beyond the DNA helix diameter. Earlier fluorescence studies support partial exposure of the BP moiety to solvent (47). Clearly, other stereoisomers of BPDE will form covalent adducts that will exhibit their own characteristic conformational features. Their structures can also be approached by the NMR techniques described in this paper and, if diffracting crystals become available, by x-ray techniques as well. Such comprehensive studies on BP and other polycyclic aromatic hydrocarbon diol epoxide adducts should provide the molecular basis for an understanding of a stereoisomer-dependent spectra of mutagenic and carcinogenic activities by these extremely important environmental genotoxins.

D.J.P. acknowledges many helpful discussions with Prof. Dezider Grunberger and Dr. Leo van Houte on the general subject of polycyclic aromatic hydrocarbon diol epoxide adducts with DNA. N.E.G. is grateful to Profs. R. G. Harvey and S. Amin for gifts of (+)-*anti*-BPDE during the development of the adduct synthesis. Computations were carried out on the Cray supercomputers at the Department of Energy's National Energy Research Supercomputer Center and the National Science Foundation's San Diego Supercomputing Center. This research was supported by Columbia University Start-Up Funds to D.J.P., by National Institutes of Health Grant CA-20851 and Department of Energy Grant DE-FG02-88ER60405 to N.E.G., by National Institutes of Health Grant DK-38676 to D.L., by National Institutes of Health Grant CA-28038, Department of Energy Grant DE-FG02-90ER60931, National Science Foundation Grant DMB-8416009 to S.B. and by Department of Energy Contract DE-AC05-840R21400 with Martin-Marietta Energy Systems to B.E.H.

1. Singer, B. & Grunberger, D. (1983) *Molecular Biology of Mutagens and Carcinogens* (Plenum, New York).
2. Basu, A. & Essigman, J. M. (1988) *Chem. Res. Toxicol.* **1**, 1–18.
3. Conney, A. H. (1982) *Cancer Res.* **42**, 4875–4917.
4. Marshall, C. J., Vousden, K. H. & Phillips, D. H. (1984) *Nature (London)* **310**, 586–589.
5. Barbacid, M. (1986) *Carcinogenesis* **7**, 1037–1042.
6. Weinberg, R. A. (1989) *Cancer Res.* **49**, 3713–3721.
7. Lawley, P. D. (1989) *Mutat. Res.* **213**, 3–25.
8. Weinstein, I. B. (1988) *Cancer Res.* **48**, 4135–4143.
9. Loeb, L. (1989) *Cancer Res.* **49**, 5489–5496.
10. Loechler, E. L. (1989) *Biopolymers* **28**, 909–927.
11. Dipple, A. (1985) in *Polycyclic Hydrocarbons and Carcinogenesis*, ACS Symposium Series, ed. Harvey, R. G. (Am. Chem. Soc., Washington), Vol. 283, pp. 1–17.
12. Slaga, T. J., Bracken, W. J., Gleason, G., Levin, W., Yagi, H., Jerina, D. M. & Conney, A. H. (1979) *Cancer Res.* **39**, 67–71.
13. Buening, M. K., Wislocki, P. G., Levin, W., Yagi, H., Thakker, D. R., Akagi, H., Koreeda, M., Jerina, D. M. & Conney, A. H. (1978) *Proc. Natl. Acad. Sci. USA* **75**, 5358–5361.
14. Chen, R. H., Maher, V. M. & McCormick, J. J. (1990) *Proc. Natl. Acad. Sci. USA* **87**, 8680–8684.
15. Brookes, P. & Osborne, M. R. (1982) *Carcinogenesis* **3**, 1223–1226.
16. Stevens, C. W., Bouck, N., Burgess, J. A. & Fahl, W. E. (1985) *Mutat. Res.* **152**, 5–14.
17. Wood, A. W., Chang, R. L., Levin, W., Yagi, H., Thakker, D. R., Jerina, D. M. & Conney, A. H. (1979) *Biochem. Biophys. Res. Commun.* **77**, 1389–1396.
18. Harvey, R. G. & Geacintov, N. E. (1987) *Acc. Chem. Res.* **21**, 66–73.
19. Geacintov, N. E. (1988) in *Polycyclic Aromatic Hydrocarbon Carcinogenesis: Structure-Activity Relationships*, eds. Yang, S. K. & Silverman, B. D. (CRC, Boca Raton, FL), Vol. 2, pp. 181–206.
20. Graslund, A. & Jernstrom, B. (1989) *Q. Rev. Biophys.* **22**, 1–37.
21. Jeffrey, A. M., Jennette, K. W., Blobstein, S. H., Weinstein, I. B., Beland, F. A., Harvey, R. G., Kasai, H., Miura, I. & Nakanishi, K. (1976) *J. Am. Chem. Soc.* **98**, 5714–5715.
22. Koreeda, M., Moore, P. D., Yagi, H., Yeh, H. J. & Jerina, D. M. (1976) *J. Am. Chem. Soc.* **98**, 6720–6722.
23. Meehan, T., Straub, K. & Calvin, M. (1977) *Nature (London)* **269**, 725–727.
24. Cosman, M., Ibanez, V., Geacintov, N. E. & Harvey, R. G. (1990) *Carcinogenesis* **11**, 1667–1672.
25. Cosman, M. (1991) Dissertation (New York Univ., New York).
26. Cheng, S. C., Hilton, B. D., Roman, J. M. & Dipple, A. (1989) *Chem. Res. Toxicol.* **2**, 334–340.
27. van de Ven, F. J. & Hilbers, C. W. (1988) *Eur. J. Biochem.* **178**, 1–38.
28. Patel, D. J., Shapiro, L. & Hare, D. (1987) *Q. Rev. Biophys.* **20**, 35–112.
29. Hingerty, B. E., Figueroa, S., Hayden, T. & Broyde, S. (1989) *Biopolymers* **28**, 1195–1222.
30. Norman, D., Abuaf, P., Hingerty, B. E., Live, D., Grunberger, D., Broyde, S. & Patel, D. J. (1989) *Biochemistry* **28**, 7462–7476.
31. Schlick, T., Hingerty, B. E., Peskin, C. S., Overton, M. L. & Broyde, S. (1990) in *Theoretical Chemistry and Molecular Biophysics*, eds. Beveridge, D., Live, D. & Lavery, R. (Academic, New York), pp. 39–58.
32. Singh, S. B., Hingergy, B. E., Singh, U. C., Greenberg, J. P., Geacintov, N. E. & Broyde, S. (1991) *Cancer Res.* **51**, 3482–3492.
33. Hare, D. R., Wemmer, D. E., Chou, S. H., Drobny, G. & Reid, B. R. (1983) *J. Mol. Biol.* **171**, 319–336.
34. Neidle, S., Subbiah, A., Kuroda, R. & Cooper, C. S. (1982) *Cancer Res.* **42**, 3766–3768.
35. Eriksson, M., Norden, B., Jernstrom, B. & Graslund, A. (1988) *Biochemistry* **27**, 1213–1221.
36. Roche, C. J., Jeffrey, A. M., Mao, B., Alfano, A., Kim, S. K., Ibanez, V. & Geacintov, N. E. (1991) *Chem. Res. Toxicol.* **4**, 311–317.
37. Dickerson, R. E., Kopka, M. L. & Drew, H. R. (1983) in *Conformation in Biology*, eds. Srinivasan, R. & Sarma, R. (Adenine, Guilderland, NY), pp. 227–257.
38. Geacintov, N. E., Gagliano, A., Ivanovic, V. & Weinstein, I. B. (1978) *Biochemistry* **17**, 5256–5262.
39. Drinkwater, N., Miller, J. A., Miller, E. C. & Yang, N. C. (1978) *Cancer Res.* **38**, 3247–3255.
40. Hogan, M. E., Dattagupta, N. & Whitlock, J. P., Jr. (1981) *J. Biol. Chem.* **256**, 4504–4513.
41. Weston, A., Newman, M. J., Mann, D. L. & Brooks, B. R. (1990) *Carcinogenesis* **11**, 859–864.
42. Aggarval, A. K., Islam, S. A. & Neidle, S. (1983) *J. Biomol. Struct. Dyn.* **1**, 873–881.
43. Anderson, R. W., Whitlow, M. D., Teether, M. M. & Mohr, S. C. (1987) *J. Biomol. Struct. Dyn.* **5**, 383–404.
44. Rao, S. N., Lybrand, T., Michaud, D., Jerina, D. M. & Kollman, P. A. (1989) *Carcinogenesis* **10**, 27–38.
45. Krugh, T. R., Graves, D. E. & Stone, M. P. (1989) *Biochemistry* **28**, 9988–9994.
46. Boyd, F. L., Cheatham, S. F., Remers, W., Hill, G. C. & Hurley, L. H. (1990) *J. Am. Chem. Soc.* **112**, 3279–3289.
47. Geacintov, N. E., Zinger, D., Ibanez, V., Santella, R., Grunberger, D. & Harvey, R. G. (1987) *Carcinogenesis* **8**, 925–935.